East European Journal of Physics. 2. 369-382 (2025)
DOI:10.26565/2312-4334-2025-2-46 ISSN 2312-4334

EXACT ANALYSIS OF DIFFUSION-THERMO EFFECT ON MHD NATURAL CONVECTIVE FLOW PAST AN OSCILLATING VERTICAL PLATE WITH CHEMICAL REACTION AND THERMAL RADIATION IN POROUS MEDIUM

Dibya Jyoti Saikia[a]*, Nazibuddin Ahmed[b], Richa Deb Dowerah[c], Ardhendu Kumar Nandi[a], Rajdeep Bordoloi[d], Harun Al Rashid[e]

[a]*Department of Mathematics, Basugaon College, Basugaon, BTR, Chirang,783372, India*
[b]*Department of Mathematics Cotton University, Guwahati, 781001, India*
[c]*Department of Mathematics, Gauhati University, Guwahati, Assam, 781014, India*
[d]*Department of Mathematics, Sibsagar University, Sibsagar, Assam, 785640, India*
[e]*Department of Mathematics, Bilasipara College, Bilasipara, 783348, India*
**Corresponding Author e-mail: dssaikia18@gmail.com*
Received September 21, 2024; revised January, 3, 2025; in final form March 1, 2025; accepted May 21, 2025

The primary goal of this investigation is to explore the impact of diffusion-thermo on the flow characteristics of MHD natural convection via a permeable medium past an infinitely oscillating upright plate, while accounting for chemical reaction and thermal radiation effects. The Laplace transformation approach is employed to solve the governing equations for species continuity equation, energy and momentum. The simulation findings show that thermal radiation increases the primary fluid velocity while decreasing the secondary fluid velocity. Furthermore, increasing the Dufour number (Du) results in higher temperature fields as well as an increase in both primary and secondary fluid velocities. Also, the diffusion-thermo effect contributes to improve the temperature field. The equation for skin friction is obtained and graphically shown. Three-dimensional surface plots are used to demonstrate the Nusselt and Sherwood numbers. In addition, graphical representations are used to portray the effect of non-dimensional factors on concentration, temperature, and velocity patterns.
Keywords: *Free convection; Porous medium; Diffusion-thermo; Chemical reaction; Thermal radiation*
PACS: 44.25.f, 44.30.v, 44.40 a, 47.65.d

1. INTRODUCTION

A "porous medium" is a system composed of solid entities with interconnected or related voids. Flow via permeable media is crucial in numerous applications, including crude oil recovery, large-scale chemical reactions which involves adsorbents, filters and catalysts, geophysical phenomena and mineral extraction. Important uses for flow via permeable medium were fully studied in comprehensive research by Alazmi and Vafai [1]. Geophysics, oil recovery techniques, metal processing, die filling, agricultural and industrial water distribution are among the applications. Alazmi and Vafai's research gives important insights into the broad and practical ramifications of porous media flow in a variety of industries and scientific areas. In the presence of a porous inner spinning cylinder, Lahonian et al. [2] investigated the mixed convection of several nanofluids. Haritha et al. [3] discussed the mass and heat transport of magnetohydrodynamics Jeffrey nanofluid flow via a permeable medium, through an inclined plate when Soret effects, radiation and chemical reaction are taken into account. Jauhri and Mishra [4] investigated MHD nanofluid flow across a stretching sheet numerically and in the existence of porous media and including the second-order velocity slip effect. The investigation of mass and heat transport upon unsteady magnetohydrodynamic flow across an endless vertically oscillating permeable plate was conducted by Krishna et al. [5].

Because of its numerous uses in scientific and technical domains, there has been a surge in interest in investigating heat and mass transport processes involving free convection through porous surfaces in recent years. Natural convection, driven simply by density differences caused by temperature gradients and without any external factors, has received a lot of attention. For example, Matta et al. [6] investigated the influence of viscous dissipation upon MHD natural convection flow via a semi-infinite vertically movable permeable sheet in presence of heat sink and chemical reaction. Meanwhile, Hamad [7] investigated the unsteady MHD natural convective flow via a vertically endless permeable plate in the presence of radiation absorption effects. In a distinct line of research, in the presence of hall and ion-slip currents, Singh et al. [8] examined how a rotating fluid's MHD free convective flow is affected by time-varying wall temperature and concentration. In addition, recent studies by other researchers, such as Nabway et al. [9], Saha et al. [10], and Saikia et al. [11], have focused on the use of free convection in their respective studies.

The energy flux generated inside a chemical structure due to composition gradients is known as the Dufour effect. When a notable concentration gradient leads to a heat flux, it presents an inverse phenomenon to thermal diffusion and this effect is often termed as Dufour effect. In their research, Goud et al. [12] examined the impacts of Soret, Dufour and chemical reaction on MHD heat transfer of a Casson fluid over an exponentially permeable stretching surface with slip effects. Additionally, Sekhar et al. [13] investigated the influence of radiative heat sources on fluid flow in the presence

Cite as: D.J. Saikia, N. Ahmed, R.D. Dowerah, A.K. Nandi, R. Bordoloi, H. Al Rashid, East Eur. J. Phys. 2, 369 (2025), https://doi.org/10.26565/2312-4334-2025-2-46

of Soret and Dufour effects for MHD Casson nanofluid over a stretching surface. Meanwhile, Deepika et al. [14] explored the Soret and Dufour effects on MHD mixed convection flow of a Casson hybrid nanofluid over a permeable stretching sheet. Moreover, Choudhary et al. [15] studied the thermal diffusion and diffusion thermo effects in a three-dimensional MHD flow via a semi-infinite vertical plate in the presence of constant heat flux.

Radiation is the electromagnetic transport of heat. Currently, many researchers are using radiation to examine the issues connected with MHD natural convective heat and mass movement in a variety of industrial operations such as archaeology, astronomy, space exploration, energy generation, aeronautics, and radioactive fluxes. In one work, Reddy and Goud [16] looked at how thermal radiation affected the flow of MHD nanofluid across an endless vertical flat plate. Bejwada and Nadeppanavar [17] investigated the influence of thermal radiation on magnetohydrodynamic heat transfer in a micropolar fluid flow over a vertical moving porous plate. Meanwhile, Algehyne et al. [18] investigated the combined effects of thermal radiation and suction/injection on magnetohydrodynamic hybrid nanofluid flow past a convectively heated stretching surface. Furthermore, Koli and Salunkhe [19] have investigated the effects of magnetic fields and thermal radiation on the flow of MHD nanofluids over a stretched sheet.

Chemical reactions, as opposed to physical or nuclear processes, involve the rearrangement of a substance's ionic structure. Chemical reactions are classified as heterogeneous or homogeneous based on whether they occur at an interface or in a single-phase volume. Vijay and Sharma [20] investigated the effect of chemical reaction and thermal radiation on entropy generation analysis in MHD hybrid nanofluid flow. Similarly, Iranian et al. [21] studied the effect of heat generation on Magnetohydrodynamic Powell-Eyring fluid flow along a vertical surface using a chemical reaction. Meanwhile, Omar et al. [22] studied the impacts of thermal radiation and chemical reaction on unsteady magnetohydrodynamics Casson fluid flow in the existence of a porous material. Moreover, additional researchers, including Reddy et al. [23], Appidi et al. [24], have also undertaken their research involving chemical reactions.

In this paper, the impact of the Dufour number, chemical reaction, and heat radiation on the unsteady free convective Newtonian flow through a porous medium employing an indefinitely oscillating vertical plate is investigated. For the flow model, an exact solution for velocity, temperature and concentration profiles is achieved. The novelty of the current investigation is that, in addition to thermal radiation, both diffusion-thermo and a first-order homogeneous chemical reaction are taken into consideration. This research is highly relevant in technical applications, including solar energy collection systems, catalytic reactors, material processing, nuclear waste storage facilities, and petroleum product and gas recovery.

2. MATHEMATICAL FORMULATION AND GEOMETRICAL SETUP FOR THE FLOW PROBLEM

To establish a rectangular Cartesian coordinate system, the x'-axis is aligned vertically upward along the plate's length, while the y'-axis is aligned across the plate's breadth. The z'-axis is perpendicular to the plate. Figure 1 provides a visual representation of the geometric arrangement, illustrating the effects of Dufour number upon the flow characteristics of MHD free convection through a porous medium past an oscillating vertical plate. This analysis incorporates factors such as chemical reaction and thermal radiation. Initially, the fluid and the plate are assumed to maintain a consistent temperature and concentration both on the fluid's surface and within its interior. As time progresses beyond $t' > 0$, the plate experiences rotational motion within its own plane, with a certain velocity $U_o e^{i\Lambda\omega t'}$. Additionally, the plate's temperature and concentration may vary, either increasing or decreasing to values denoted as $T' = T'_{\infty} + (T'_w - T'_{\infty})\Lambda t'$ and $C' = C'_{\infty} + (C'_w - C'_{\infty})\Lambda t'$ respectively. Since the flow possesses an extremely low Reynolds number, the influence of magnetic fields and viscous dissipation is considered insignificant. In this particular flow scenario, the fluid is characterized as "gray," indicating its ability to absorb and emit radiation without scattering light. A uniform transverse magnetic field B_o is applied in the z' direction, perpendicular to the plate. The unsteady flow, subject to the conventional Boussinesq approximation, is governed by a set of equations that are subsequently analyzed.

Momentum equation:

$$\frac{\partial u'}{\partial t'} = \nu \frac{\partial^2 u'}{\partial z'^2} + g\beta'(T' - T'_{\infty}) + g\overline{\beta}(C' - C'_{\infty}) - \left(\frac{\sigma B^2{}_o}{\rho} + \frac{\nu}{K'}\right) u', \tag{1}$$

$$\frac{\partial v'}{\partial t'} = \nu \frac{\partial^2 v'}{\partial z'^2} - \left(\frac{\sigma B^2{}_o}{\rho} + \frac{\nu}{K'}\right) v'. \tag{2}$$

Energy equation:

$$\frac{\partial T'}{\partial t'} = \frac{\kappa}{\rho C_p}\frac{\partial^2 T'}{\partial z'^2} - \frac{1}{\rho C_p}\frac{\partial q'_r}{\partial z'} + \frac{D_M K_T}{C_p C_S}\frac{\partial^2 C'}{\partial z'^2}. \tag{3}$$

Species continuity equation:

$$\frac{\partial C'}{\partial t'} = D_M \frac{\partial^2 C'}{\partial z'^2} + \overline{k}(C' - C'_{\infty}). \tag{4}$$

The velocity, temperature, and concentration fields are subject to the following relevant initial and boundary conditions:

$$\left.\begin{array}{l} u'=0,\ v'=0,\ T'=T'_{\infty},\ C'=C'_{\infty},\ t'\le 0,\ \forall z' \\ u'=U_o\, e^{i\Lambda\omega t'},\ v'=0,\ T'=T'_{\infty}+(T'_w-T'_{\infty})\Lambda t',\ C'=C'_{\infty}+(C'_w-C'_{\infty})\Lambda t',\ for\ t'>0,\ z'=0 \\ u'\to 0,\ v'\to 0,\ T'\to T'_{\infty},\ C'\to C'_{\infty}\quad for\ \ t'>0,\ as\ z'\to\infty \end{array}\right\}. \tag{5}$$

Equations (1) and (2) can be coupled using the complex integer q = u + iv, yielding:

$$\frac{\partial q'}{\partial t'}=\frac{\partial u'}{\partial t'}+i\,\frac{\partial v'}{\partial t'},$$

$$or \tag{6}$$

$$\frac{\partial q'}{\partial t'}=\nu\frac{\partial^2 q'}{\partial z'^2}+g\,\beta'(T'-T'_{\infty})+g\,\overline{\beta}(C'-C'_{\infty})+\left(\frac{\sigma B^2{}_o}{\rho}+\frac{\nu}{K'}\right)q'.$$

In an optically thin, grey gas scenario, the expression for the rate of local radiation absorption is as follows:

$$\frac{\partial q'_r}{\partial z'}=-4a'\sigma'(T'^4_{\infty}-T'^4). \tag{7}$$

The absolute value of $|T'-T'_{\infty}|$ tends to zero as the temperature differential between the boundary layer and the region furthest from the plate becomes minimal. The following result is obtained by expanding the term T'^4 in a Taylor series with respect to the free stream temperature T'_{∞}:

$$T'^4\cong 4T'^3_{\infty}T'-3T'^4_{\infty}. \tag{8}$$

By using equations (7) and (8) concurrently, the term $\frac{\partial q'_r}{\partial z'}$ in equation (3) can be eliminated, resulting in the transformation of equation (3) into:

$$\frac{\partial T'}{\partial t'}=\frac{\kappa}{\rho C_p}\frac{\partial^2 T'}{\partial z'^2}-\frac{16\,a'\sigma'T'^3_{\infty}}{\rho\,C_p}(T'-T'_{\infty})+\frac{D_M K_T}{C_p C_S}\frac{\partial^2 C'}{\partial z'^2}. \tag{9}$$

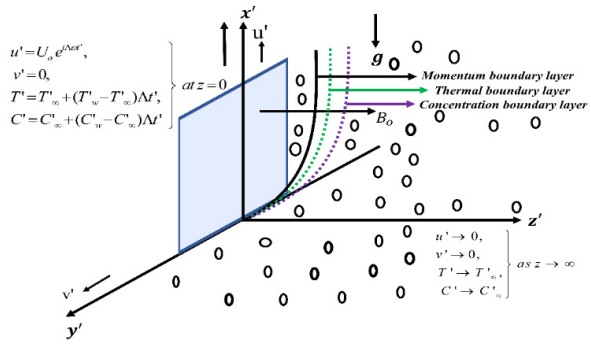

Figure 1. Geometrical configuration of the flow problem

Introducing the non-dimensional parameters:

$$\left.\begin{array}{l} z=\dfrac{U_o z'}{\nu},\ q=\dfrac{q'}{U_o},\ T=\dfrac{T'-T'_{\infty}}{T'_w-T'_{\infty}},\ C=\dfrac{C'-C'_{\infty}}{C'_w-C'_{\infty}}, \\ Sc=\dfrac{\nu}{D_M},\ \Pr=\dfrac{\rho\nu C_p}{\kappa},\ K'=\dfrac{U^2{}_o K}{\nu^2},\ \Lambda=\dfrac{U^2{}_o}{\nu},\ Du=\dfrac{D_M D_T(C'_w-C'_{\infty})}{\nu C_p C_s(T'_w-T'_{\infty})} \\ Gr=\dfrac{\nu g\,\beta'(T'_w-T'_{\infty})}{U^3{}_o},\ k=\dfrac{\overline{k}\nu}{U^2{}_o},\ Gm=\dfrac{\nu g\,\overline{\beta}\,(C'_w-C'_{\infty})}{U^3{}_o}, \\ t'=\dfrac{U^2{}_o t}{\nu},\ M=\dfrac{\sigma B^2{}_o\nu}{\rho U^2{}_o},\ R=\dfrac{16\,a'\sigma'T'^3_{\infty}\nu^2}{\kappa U^2{}_o} \end{array}\right\}. \tag{10}$$

Equations (6), (4), and (9) undergo a transformation when the non-dimensional parameters indicated in equation (10) are applied, yielding:

$$\frac{\partial q}{\partial t}=\frac{\partial^2 q}{\partial z^2}+Gr\,T+Gm\ C-\xi\,q. \tag{11}$$

Where, $\xi = M + (1/k)$.

$$\frac{\partial C}{\partial t} = \frac{1}{Sc}\frac{\partial^2 C}{\partial z^2} - k\,C. \tag{12}$$

$$\frac{\partial T}{\partial t} = \frac{1}{\Pr}\frac{\partial^2 T}{\partial z^2} - \frac{R}{\Pr}T + Du\frac{\partial^2 C}{\partial z^2}. \tag{13}$$

Equations (11), (12), and (13) exhibit dimensionless formulations of the momentum, concentration, and energy equations, respectively. Furthermore, we derive analogous dimensionless initial and boundary conditions which are shown below:

$$\left.\begin{array}{l} q = 0,\ T = 0,\ C = 0,\ t \le 0,\ \forall z \\ q = e^{i\omega t},\ T = t,\ C = t,\ t > 0,\ at\ z = 0 \\ q \to 0,\ T \to 0,\ C \to 0,\ t > 0,\ as\ z \to \infty \end{array}\right\}. \tag{14}$$

3. SOLUTION OF THE FLOW PROBLEM

Using the Laplace transformation method, the system of interconnected partial differential equations provided by equations (11)-(13) was successfully solved. Furthermore, the study took into account the insertion of the boundary conditions shown in equation (14). The Laplace transformation of equations (11), (12), and (13) yielded the following results:

The application of the Laplace transformation to equation (12) yields:

$$\frac{d^2\overline{C}}{dz^2} - Sc\,(s+k)\,\overline{T} = 0. \tag{15}$$

With the implementation of the Laplace transformation, the corresponding boundary conditions were modified to,

$$\begin{array}{l} \overline{C} = \dfrac{1}{s^2}\ at\ z = 0 \\ \overline{C} \to 0, as\ z \to \infty \end{array} \tag{16}$$

The fluid concentration solution is then obtained in the format shown below by applying the inverse Laplace transformation to equation (15) and taking into account the boundary condition supplied in equation (16).

$$\phi = f_1 = f(Sc, k,\ z,\ t). \tag{17}$$

Again, upon performing the Laplace transformation on equation (13), we obtain-

$$\frac{d^2\overline{T}}{dz^2} - (s\,\Pr + R)\,\overline{T} = -\frac{Du\,Sc\,\Pr}{s^2}(k+s)e^{-\sqrt{Sc}\sqrt{k+s}\,z}, \tag{18}$$

With the implementation of the Laplace transformation, the corresponding boundary conditions were modified to,

$$\begin{array}{l} \overline{T} = \dfrac{1}{s^2}\ at\ z = 0 \\ \overline{T} \to 0, as\ z \to \infty \end{array} \tag{19}$$

The fluid temperature solution is then obtained in the format shown below by applying the inverse Laplace transformation to equation (18) and taking into account the boundary condition supplied in equation (19).

$$\theta = (1 - B_1 A_2) f_2 + B_1 A_2 f_3 - D_1\psi_1 + D_2\psi_2 + D_1\psi_3 - D_2\psi_4 \tag{20}$$

Where,

$$\psi_1 = \psi(\beta,\ R\beta,\ z,\ t),\ \psi_2 = \psi(\beta,\ R\beta - B_2,\ z,\ t),$$
$$\psi_3 = \psi(Sc,\ k,\ z,\ t),\ \psi_4 = \psi(Sc,\ k - B_2,\ z,\ t),$$
$$f_2 = f(\beta,\ R\beta,\ z,\ t),\ f_3 = f(Sc,\ k,\ z,\ t),\ \beta = \frac{1}{\Pr},\ B_1 = -\frac{Du\,Sc\,\Pr\,k}{Sc - \Pr},$$
$$B_2 = \frac{Sc\ k - R}{Sc - \Pr},\ B_3 = -\frac{Du\,Sc\,\Pr}{Sc - \Pr},\ A_1 = -\frac{1}{B^2{}_2},\ A_2 = \frac{1}{B_2},\ A_3 = \frac{1}{B^2{}_2}$$

Upon performing the Laplace transformation on equation (11), we obtain:

$$\frac{d^2\,\bar{q}}{dz^2}-(s+\xi)\bar{q}=-Gr\bar{T}-Gm\bar{C}, \tag{21}$$

The boundary conditions undergo modifications as a result of executing the Laplace transformation, taking the following form:

$$\begin{aligned}&\bar{q}=\frac{1}{s-i\omega}\ at\ z=0\\&\bar{q}\to 0, as\ z\to\infty.\end{aligned} \tag{22}$$

Finally, the solution for fluid velocity is produced in the following format by adding the boundary condition indicated in equation (22) and applying the inverse Laplace transformation of equation (21).

$$q=q_1-q_2-q_3-q_4-q_5-q_6-q_7+q_8+q_9+q_{10}+q_{11}+q_{12}+q_{13}\,. \tag{23}$$

Where,

$q_1=e^{i\omega t}\,h(\delta+i\omega,\,z,\,t)=h_1,$

$q_2=G_1K_1\,h_2+G_1K_2\,F_1+G_1K_3\,h_3,$

$q_3=G_3L_1\,h_2+G_3L_2\,F_1+G_3L_3\,h_4+G_3L_4\,h_3,$

$q_4=G_4L_2\,h_2+G_4N_1\,h_4+G_4N_2\,h_3,$

$q_5=G_5P_1\,h_2+G_5P_2\,F_1+G_5P_3\,h_4+G_5P_4\,h_5,$

$q_6=G_7P_2\,h_2+G_7Q_1\,h_4+G_7Q_2\,h_5,$

$q_7=G_8I_1\,h_2+G_8I_2\,F_1+G_8I_3\,h_5,$

$q_8=G_1K_1\,\psi_1+G_1K_2\,f_2+G_1K_3\,\psi_5,$

$q_9=G_3L_1\,\psi_1+G_3L_2\,f_2+G_3L_3\,\psi_2+G_3L_4\,\psi_5,$

$q_{10}=G_4L_2\,\psi_1+G_4N_1\,\psi_2+G_4N_2\,\psi_5,$

$q_{11}=G_5P_1\,\psi_3+G_5P_2\,f_3+G_5P_3\,\psi_4+G_5P_4\,\psi_6,$

$q_{12}=G_7P_2\,\psi_2+G_7Q_1\,\psi_4+G_7Q_2\,\psi_6,$

$q_{13}=G_8I_1\,\psi_3+G_8I_2\,f_3+G_8I_3\,\psi_6,$

$G_1=-\frac{Gr}{\beta-1},\ G_2=\frac{R\beta^2-\xi}{\beta-1},\ G_3=\frac{GrB_1}{\beta-1},$

$G_4=\frac{GrB_3}{\beta-1},\ G_5=-\frac{GrB_1}{Sc-1},\ G_6=\frac{Sc\,k-\xi}{Sc-1},$

$G_7=-\frac{Gr\,B_3}{Sc-1},\ G_8=-\frac{Gm}{Sc-1},$

$K_1=-\frac{1}{G^2{}_2},\ K_2=\frac{1}{G_2},\ K_3=\frac{1}{G^2{}_2},$

$L_1=-\left(\frac{B_2+G_2}{B^2{}_2\,G^2{}_2}\right),\ L_2=\frac{1}{B_2G_2},\ L_3=-\frac{1}{B^2{}_2\left(B_2-G_2\right)},\ L_4=\frac{1}{G^2{}_2\left(B_2-G_2\right)},$

$N_1=\frac{1}{B_2\left(B_2-G_2\right)},\ N_2=-\frac{1}{G_2\left(B_2-G_2\right)},$

$P_1=-\left(\frac{B_2+G_6}{B^2{}_2\,G^2{}_6}\right),\ P_2=\frac{1}{B_2G_6},\ P_3=-\frac{1}{B^2{}_2\left(B_2-G_6\right)},\ P_4=\frac{1}{G^2{}_6\left(B_2-G_6\right)},$

$Q_1=\frac{1}{B_2\left(B_2-G_6\right)},\ Q_2=-\frac{1}{G_6\left(B_2-G_6\right)},$

$I_1=-\frac{1}{G^2{}_6},\ I_2=\frac{1}{G_6},\ I_3=\frac{1}{G^2{}_6}.$

$h_1=e^{i\omega t}\,h(\xi+i\omega,\,z,\,t),\qquad h_2=h(\xi,\,z,\,t),$

$h_3=e^{-G_2t}h(\xi-G_2,\,z,\,t),\qquad h_4=e^{-B_2t}h(\xi-B_2,\,z,\,t),$

$h_5=e^{-G_6t}h(\xi-G_6,\,z,\,t),\qquad \psi_5=e^{-G_2t}\psi(\beta,\,R\beta-G_2,\,z,\,t),$

$\psi_6=e^{-G_6t}\,\psi(Sc,\,k-G_6,\,z,\,t),\quad F_1=F(\xi,\,z,\,t).$

3.1. Solution for skin friction

The following procedure, in accordance with Newton's law of viscosity, can be used to estimate the viscous drag per unit area at the plate.

$$\tau' = -\mu \frac{\partial q'}{\partial z'}\Big]_{z=0} = -\mu U_o \frac{\partial q}{\partial z}\frac{\partial z}{\partial z'} = -\mu U_o \frac{\partial q}{\partial z}\frac{\partial}{\partial z'}\left(\frac{U_o z'}{\nu}\right) = -\frac{\mu U_o^{\,2}}{\nu}\frac{\partial q}{\partial z}$$

The skin friction coefficient at the plate is defined as

$$\tau = \frac{\tau'}{\frac{\mu U_o^{\,2}}{\nu}} = -\frac{\partial q}{\partial z}\Big]_{z=0}$$

$$= -\frac{\partial q_1}{\partial z}\Big]_{z=0} + \frac{\partial q_2}{\partial z}\Big]_{z=0} + \frac{\partial q_3}{\partial z}\Big]_{z=0} + \frac{\partial q_4}{\partial z}\Big]_{z=0} + \frac{\partial q_5}{\partial z}\Big]_{z=0} + \frac{\partial q_6}{\partial z}\Big]_{z=0} + \frac{\partial q_7}{\partial z}\Big]_{z=0}$$
$$- \frac{\partial q_8}{\partial z}\Big]_{z=0} - \frac{\partial q_9}{\partial z}\Big]_{z=0} - \frac{\partial q_{10}}{\partial z}\Big]_{z=0} - \frac{\partial q_{11}}{\partial z}\Big]_{z=0} - \frac{\partial q_{12}}{\partial z}\Big]_{z=0} - \frac{\partial q_{13}}{\partial z}\Big]_{z=0},$$

i.e

$$\begin{aligned}
&\tau = -\hbar_1 + (D_1K_1 + G_3L_1 + G_4L_2 + G_5P_1)\,\hbar_2 + (D_1K_3 + G_3L_4 + G_4N_2)\,\hbar_3 + \\
&(G_3L_3 + G_4N_1 + G_5P_3 + G_7Q_1)\,\hbar_4 + (G_5P_4 + G_7Q_2 + G_8I_3)\,\hbar_5 + \\
&(D_1K_2 + G_3L_2 + G_5P_2 + G_8I_2)\,\Gamma_1 - (G_1K_1 + G_1L_1 + G_4L_2)\,\Omega_1 - \\
&(G_3L_3 + G_4N_1)\Omega_2 - (G_5P_1 + G_7P_2 + G_8I_1)\,\Omega_3 - \\
&(G_5P_3 + G_7Q_1)\Omega_4 - (G_1K_3 + G_3L_4 + G_4N_2)\,\Omega_5 - \\
&(G_5P_4 + G_7Q_2 + G_8I_3)\,\Omega_6 - (G_1K_2 + G_3L_2)\,\varphi_2 - \\
&(G_5P_2 + G_8I_2)\,\varphi_2.
\end{aligned} \tag{24}$$

Where,

$$\hbar_1 = \frac{\partial h_1}{\partial z}\Big]_{z=0} = e^{i\omega t}\,\hbar(\xi + i\omega, t), \qquad \hbar_2 = \frac{\partial h_2}{\partial z}\Big]_{z=0} = \hbar(\xi, t),$$

$$\hbar_3 = \frac{\partial h_3}{\partial z}\Big]_{z=0} = e^{-G_2 t}\,\hbar(\xi - G_2, t), \qquad \hbar_4 = \frac{\partial h_4}{\partial z}\Big]_{z=0} = e^{-B_2 t}\,\hbar(\xi - B_2, t),$$

$$\hbar_5 = \frac{\partial h_5}{\partial z}\Big]_{z=0} = e^{-G_6 t}\,\hbar(\xi - G_6, t), \qquad \Omega_1 = \frac{\partial \psi_1}{\partial z}\Big]_{z=0} = \Omega(\beta, R\beta, t),$$

$$\Omega_2 = \frac{\partial \psi_2}{\partial z}\Big]_{z=0} = e^{-B_2 t}\,\Omega(\beta, R\beta - B_2, t), \qquad \Omega_3 = \frac{\partial \psi_3}{\partial z}\Big]_{z=0} = \Omega(Sc, k, t),$$

$$\Omega_4 = \frac{\partial \psi_4}{\partial z}\Big]_{z=0} = e^{-B_2 t}\,\Omega(Sc, k - B_2, t), \qquad \Omega_5 = \frac{\partial \psi_2}{\partial z}\Big]_{z=0} = e^{-G_2 t}\,\Omega(\beta, R\beta - G_2, t),$$

$$\Omega_6 = \frac{\partial \psi_6}{\partial z}\Big]_{z=0} = e^{-G_6 t}\,\Omega(Sc, k - G_6, t), \qquad \varphi_2 = \frac{\partial f_2}{\partial z}\Big]_{z=0} = \varphi(\beta, R\beta, t),$$

$$\varphi_3 = \frac{\partial f_3}{\partial z}\Big]_{z=0} = \varphi(Sc, k, t), \qquad \Gamma_1 = \frac{\partial F_1}{\partial z}\Big]_{z=0} = \Gamma(\xi, t).$$

3.2. Sherwood number

The Sherwood number, which pertains to the rate of mass transfer at the plate, is computed using Fick's diffusion law. The following approach can be employed to find the mass flux M_w from the plate at z'=0:

$$M_w = -D_M \frac{\partial C'}{\partial z'}\Big]_{z'=0} = -\frac{D_M U_o \left(C'_w - C'_\infty\right)}{\nu}\frac{\partial \phi}{\partial z}\Big]_{z=0},$$

Thus, the coefficient of rate of mass transfer at the plate is,

$$Sh = \frac{M_w}{D_M U_o \left(C'_w - C'_\infty\right)} = -\frac{\partial \phi}{\partial z}\Big]_{z=0}, \quad Sh = -\frac{\partial \phi}{\partial z}\Big]_{z=0} = -\frac{\partial f_1}{\partial z}\Big]_{z=0} = \varphi_1 = \varphi(Sc, k, t).$$

3.3. Solution for Nusselt number

Estimating and comprehending the rate of heat transfer at the plate is crucial in estimating the Nusselt number. This includes computing the ratio of convective to conductive heat transfer in the fluid across the boundary. Fourier's law of conduction is utilized to calculate the heat flux Q' from the plate at z'=0 to the fluid.

$$Q' = -\kappa \frac{\partial T'}{\partial z'}\Big]_{z'=0} = -\frac{\kappa U_o \left(T'_w - T'_\infty\right)}{\nu} \frac{\partial T}{\partial z}\Big]_{z=0}.$$

The coefficient of rate of heat transfer at the plate is,

$$Nu = \frac{\nu Q'}{\kappa U_o \left(T'_w - T'_\infty\right)} = -\frac{\partial \theta}{\partial z}\Big]_{z=0} = (1 - B_1 A_1)\varphi_2 + B_1 A_1 \varphi_3 - D_1 \Omega_1 + D_2 \Omega_2 + D_1 \Omega_3 - D_2 \Omega_4.$$

4. RESULTS AND DISCUSSION

A comprehensive investigation is performed to quantitatively determine primary fluid velocity (u), secondary fluid velocity (v), temperature (θ), concentration (ϕ), rate of heat transfer (Nu), and mass transfer (Sh) to enhance the comprehension of the fluid flow phenomena. In this research endeavor, Prandtl number (Pr) and Schmidt number (Sc) are deliberately chosen to be 0.71 and 0.22, respectively, to match the properties of dry air and hydrogen at a standard pressure of 1 atmosphere. To preserve uniformity and enable comparison analysis, the variables t and R are continually assigned a fixed value of 1.2 and 1 throughout the inquiry.

Figures 2-3 demonstrate how the Schmidt number (Sc) and chemical reaction parameter (k) affect fluid concentration. Figure 2 depicts a drop in fluid concentration as the Schmidt number increases. This discovery is consistent with scientific principles, as a higher Schmidt number correlates to reduced molecule diffusivity, which accelerates concentration decline in the boundary layer.

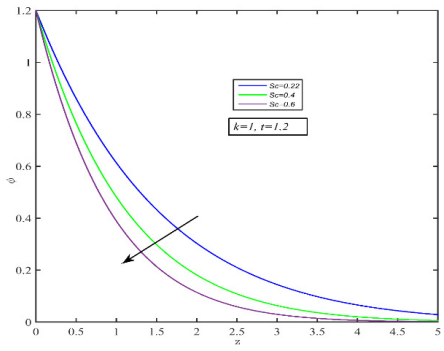

Figure 2. Concentration pattern versus distinct Sc

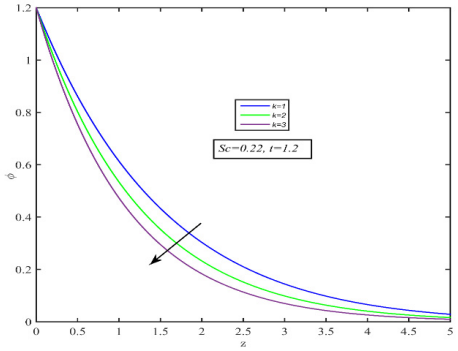

Figure 3. Concentration pattern versus distinct k

Figure 3 depicts the effect of chemical reactions on concentration patterns, exhibiting a decreasing fluid concentration as the chemical reaction parameter (k) climbs. This is due to the physical phenomena in which a rise in k causes a denser fluid, resulting in a declined concentration pattern.

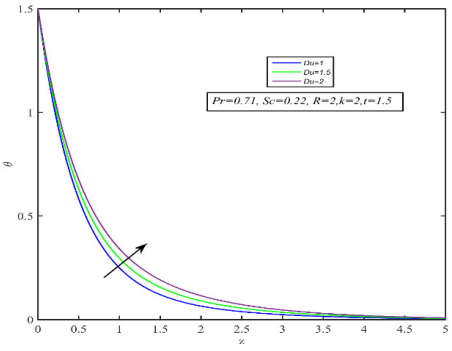

Figure 4. Temperature pattern versus distinct Du

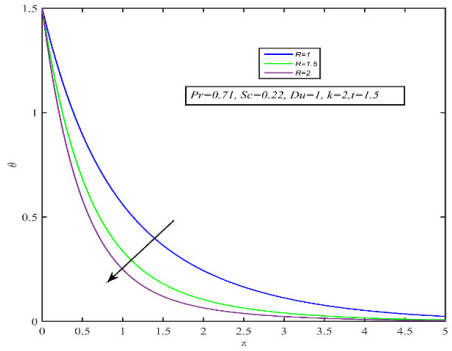

Figure 5. Temperature pattern versus distinct R

Figures 4-6 depict the temperature patterns as the Dufour number (Du), radiation parameter (R) and dimensionless time (t) are varied while the other parameters remain constant. As apparent in Figure 4, raising Du causes a boost in temperature (θ). This is due to the increased heat flux caused by the concentration gradient, which results in increased thermal stimulation in the fluid. Figure 5 shows the effect of the radiation parameter (R) on the temperature profile, indicating a considerable fall in fluid temperature as the radiation parameter increases. This discovery is related to

radiation's inhibitory effect on energy transfer to the fluid, resulting in lower temperatures. Figure 6 depicts the progressive rise in fluid temperature as dimensionless time (t) advances. Figures 7–8 showcase how the magnetic parameter (M) affects the primary velocity profile (u) and secondary velocity profile (v).

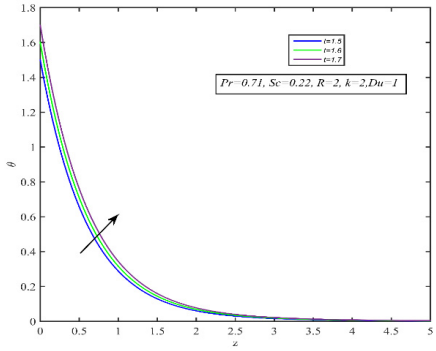

Figure 6. Temperature pattern versus distinct t

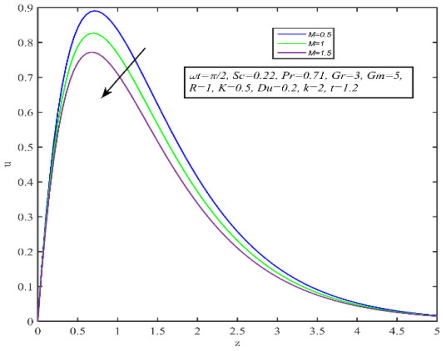

Figure 7. Primary velocity pattern (u) versus distinct M

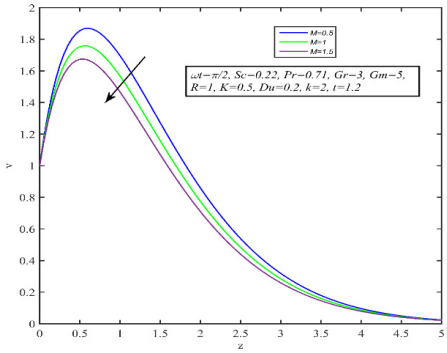

Figure 8. Secondary velocity pattern (v) versus distinct M

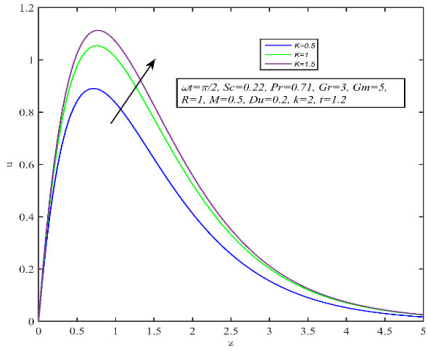

Figure 9. Primary velocity pattern (u) versus distinct K

A rise in the magnetic parameter (M) is accompanied by a decline in the velocity components u and v in both visualizations. The interaction of the magnetic field and the magnetic parameter (M) produces the Lorentz force, a magnetic body force that obstructs the velocity field. As a result, the fluid's mobility is restricted and slowed. Figures 9 and 10 show how the fluid velocity components u and v change as the permeability parameter (K) changes.

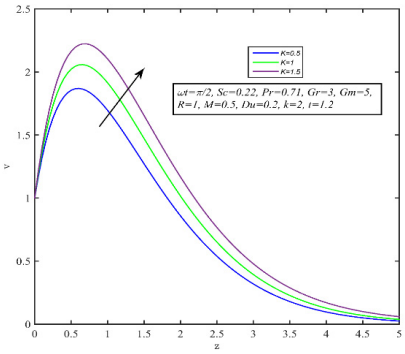

Figure 10. Secondary velocity pattern (v) versus distinct K

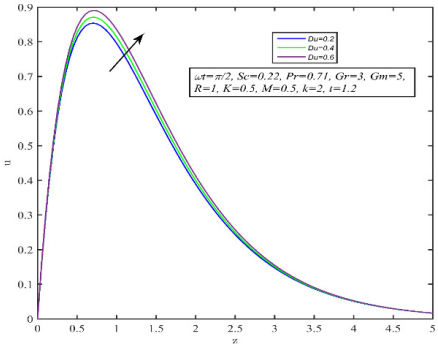

Figure 11. Primary velocity pattern (u) versus distinct Du

These graphs show that an increase in the permeability parameter (K) corresponds to an increase in the velocity components u and v. Significantly, as the permeability parameter (K) upsurges, the resistance of the flow medium reduces, resulting in quicker fluid motion in accordance with physics principles.

The relation between the velocity components u and v and the Dufour number (Du) is demonstrated in Figure 11-12. Both velocity components hike as the Dufour number (Du) grows. This discovery suggests that the fluid's velocity is accelerated as a result of the combined action of the diffusion-thermo effect and thermal buoyancy force. Physically, these factors contribute to the rise in velocity of the fluid observed in the data.

Figures 13-16 demonstrate the impact of thermal Grashof number (Gr) and solutal Grashof number (Gm) on primary and secondary velocity patterns. These graphs, spanning from 13 to 16, indicate that enhancing the thermal and solutal Grashof numbers coincides with a considerable rise in the velocity components u and v. The elevated values of Gr and Gm indicate a strengthened presence of thermal and solutal buoyancy forces near the plate, resulting in a notable acceleration of fluid motion. These empirical findings support the notion that changes in Gr and Gm have a direct effect on the fluid dynamics in the experimental setup.

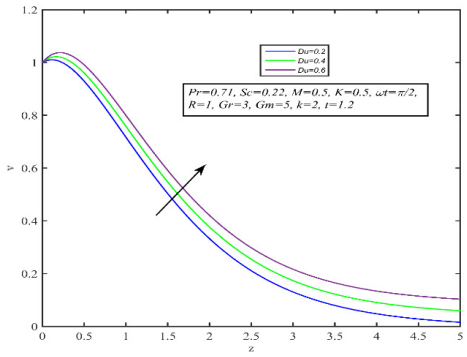

Figure 12. Secondary velocity pattern (v) versus distinct Du

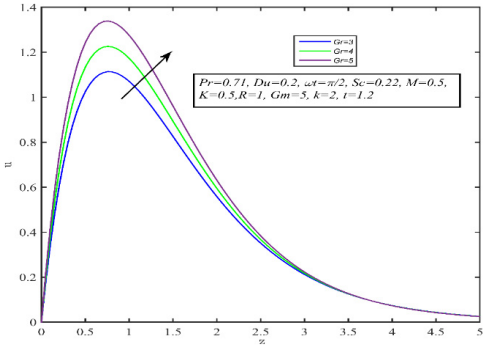

Figure 13. Primary velocity pattern (u) versus distinct Gr

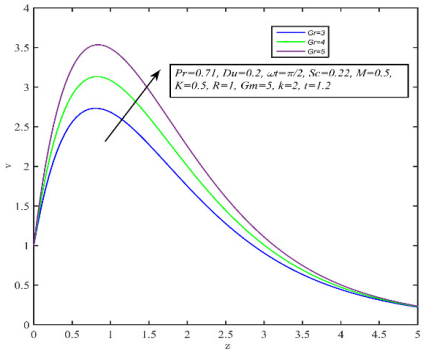

Figure 14. Secondary velocity pattern (v) versus distinct Gr

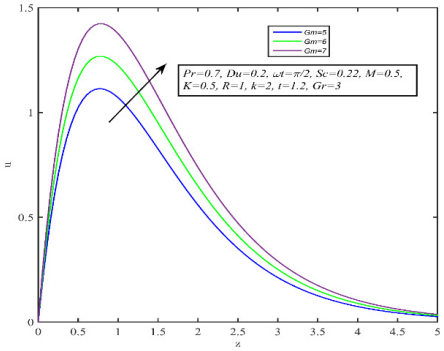

Figure 15. Primary velocity pattern (u) versus distinct Gm

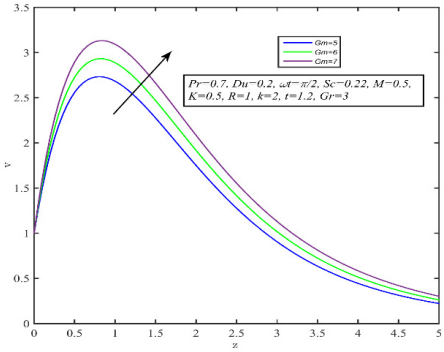

Figure 16. Secondary velocity pattern (v) versus distinct Gm

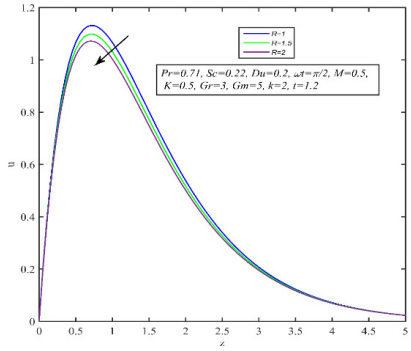

Figure 17. Primary velocity pattern (u) versus distinct R

Figures 17–18 demonstrate the influence of radiation parameter R on the velocity components u and v. Specifically, an increment in the parameter R corresponds to a decrease in the primary velocity component u, whereas it leads to a hike in the secondary velocity component v. Analysis of Figure 19 reveals that an elevation in the oscillation frequency (ωt) is associated with a reduction in the primary fluid velocity u. In contrast, Figure 20 depicts contrasting results, indicating an augmentation in the secondary fluid velocity under the same conditions. These experimental findings provide valuable insights into the impact of radiation parameter R and oscillation frequency (ωt) upon the current flow problem, contributing to a comprehensive understanding of the observed phenomena.

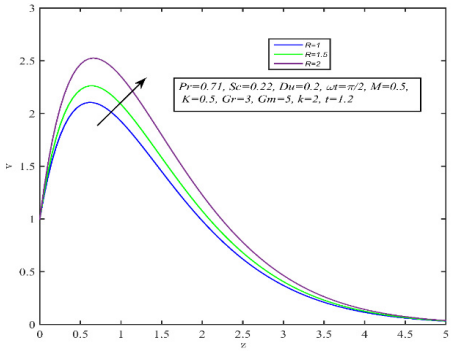

Figure 18. Secondary velocity pattern (v) versus distinct R

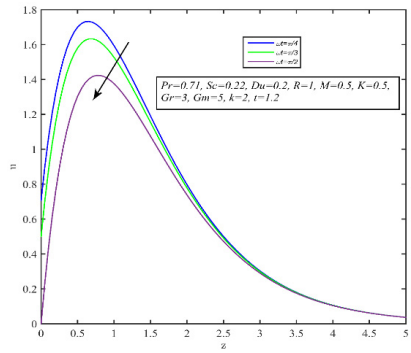

Figure 19. Primary velocity pattern (u) versus distinct ωt

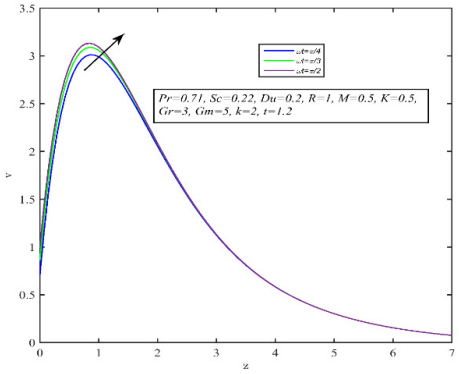

Figure 20. Secondary velocity pattern (v) versus distinct ωt

The Figures 21–24 depict the relationship between skin friction (τ) and the non-dimensional parameters Du, Gr, Gm, and R. Figures 21–23 show that elevating the Dufour number (Du), solutal Grashof number (Gr), and thermal Grashof number (Gm) enhances skin friction. Figure 24, on the other hand, shows that as the radiation parameter (R) grows, skin friction diminishes. These findings demonstrate that these non-dimensional parameters have a major impact on the skin friction phenomena, providing useful insights into the fluid flow behaviour in the investigated system.

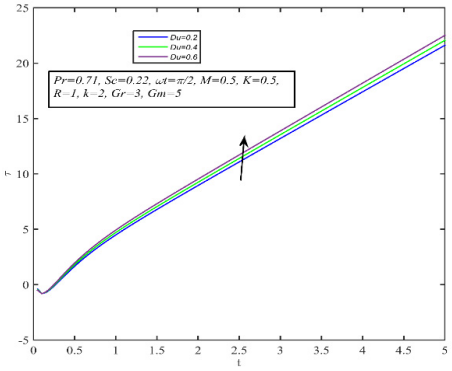

Figure 21. Skin friction (τ) vs distinct Du

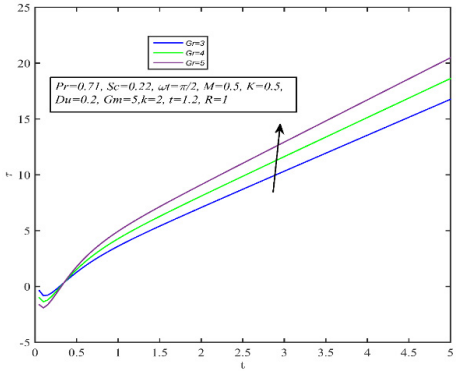

Figure 22. Skin friction (τ) vs distinct Gr

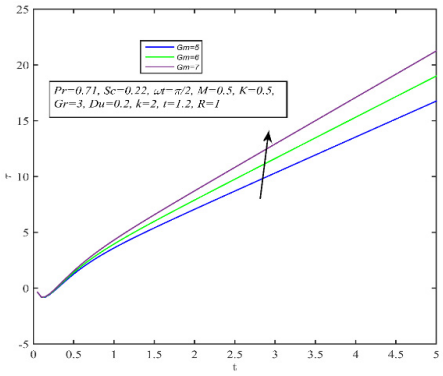

Figure 23. Skin friction (τ) vs distinct Gm

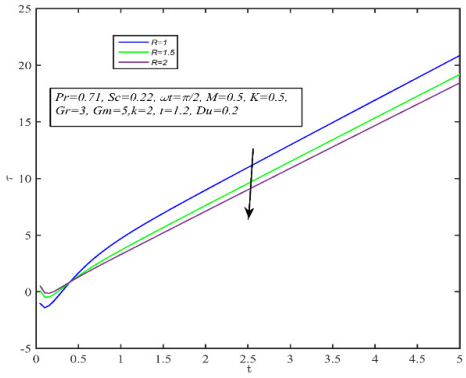

Figure 24. Skin friction (τ) vs distinct R

Surface charts are an effective visualization method for depicting the relationship between a dependent variable and two independent variables in 3D-format, allowing for a more comprehensive understanding of the data rather than individual data points. Figures 25–29 show surface plots of the Nusselt number (Nu) and Sherwood number (Sh) for various flow parameters. The Nusselt and Sherwood numbers are plotted along the z-axis, while the non-dimensional parameters Du, Pr, R, Sc, and k are plotted along the y-axis.

Figure 25 reveals that boosting the Dufour number (Du) and non-dimensional time (t) diminishes the heat transfer rate (Nu). Figure 26, on the other hand, exhibits the effect of the Prandtl number (Pr) on the Nusselt number. The heat transmission rate (Nu) declines as the Prandtl number and duration (t) rise.

Figure 27 illustrates that the rate of heat transfer (Nu) improves as the radiation parameter R and non-dimensional time (t) increase. Furthermore, both surface plots in Figures 28-29 show a significant corelation between the Sherwood number, the Schmidt number (Sc), and the chemical reaction parameter (k). As the Schmidt number and the chemical reaction parameter grow, so does the Sherwood number, which represents the mass transfer rate.

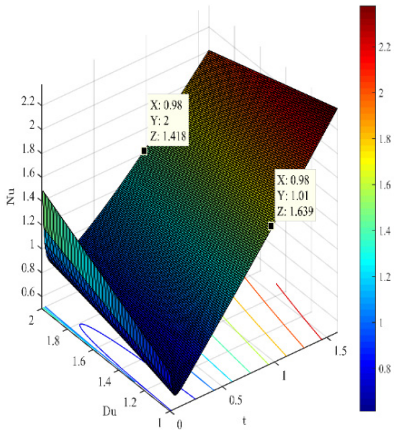

Figure 25. Nu versus Du and t

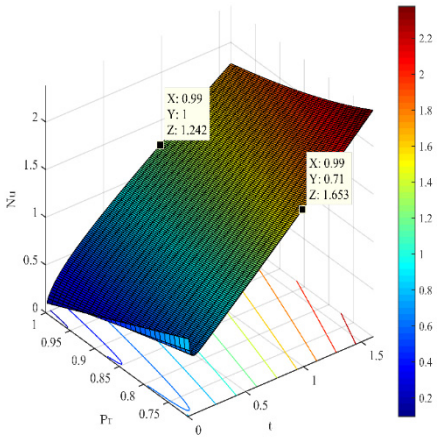

Figure 26. Nu versus Pr and t

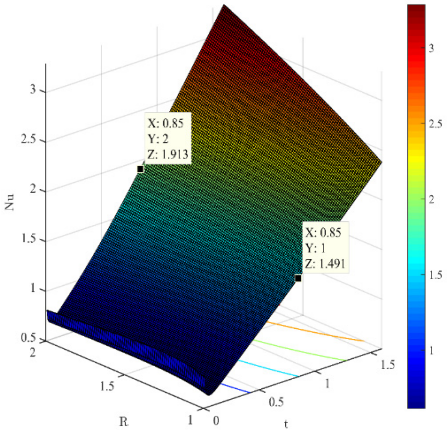

Figure 27. Nu versus R and t

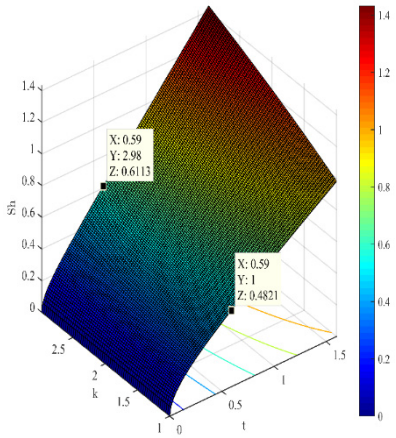

Figure 28. Sh versus Sc and t

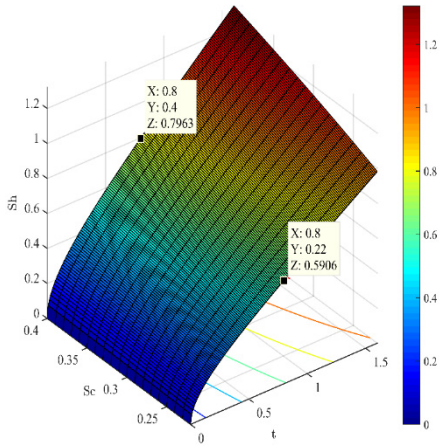

Figure 29. Sh versus k and t

5. CONCLUSIONS

This study examines the impact of diffusion-thermo on the flow characteristics of MHD free convection through a porous medium past an infinitely oscillating vertical plate, taking into account thermal radiation and chemical reaction. The investigation considers a viscous, incompressible fluid with optical properties as an optically thin grey gas, exhibiting both absorbs and emits radiation. The study yields the following key findings:

- With the increase of Dufour number, the momentum boundary layer becomes thicker significantly. As a result, it accelerates the flow.
- Higher mass diffusivity hikes the concentration field and a faster chemical reaction consumes chemical substances present in the fluid rapidly and as a result fluid concentration decline.
- The primary fluid velocity declines with rising radiation parameter R, while the secondary velocity profile shows the opposite trend, with an overall augmentation.

- An elevated radiation parameter R leads to a diminish in temperature patterns, while fluid temperature rises with higher Dufour number (Du) values. A hike in the Dufour number indicates a comprehensive rise in concentration gradient over temperature gradient. Hence increment of concentration gradient hikes the fluid temperature.
- Increased contributions of the Dufour number (Du), solutal Grashof number (Gr) and thermal Grashof number (Gm) result in increased skin friction. However, the radiation parameter R has a contrary effect, causing a decline in skin friction.
- The rates of heat transfer (Nu) decrease due to the effects of Dufour number (Du) and Prandtl number (Pr). Conversely, rates of heat transfer (Nu) accelerate when radiation parameter R hikes.
- The rate of mass transfer (Sh) increases with higher values of the chemical reaction parameter (k) and Schmidt number (Sc), respectively.

Nomenclature

Du	Dufour number	Gr	thermal Grashof number
D_M	molecular diffusivity	T'	fluid temperature
k	chemical reaction parameter	Gm	solutal Grashof number
$\vec{J}$	current density vector	v'	secondary fluid velocity in y' direction
C'_∞	concentration in the free stream	U_o	characteristic plate velocity
C_p	specific heat at constant pressure	u'	primary fluid velocity in x' direction
C'_w	concentration at the wall		**Greek Symbols**
T'_w	temperature at the wall	ν	kinematic viscosity
C_s	concentration susceptibility	σ	Stefan-Boltzman constant
T'_∞	temperature at the free stream	β'	coefficient of volumetric expansion
M	magnetic parameter	$\bar{\beta}$	coefficient of solutal expansion
q'_r	radiating heat flux	κ	thermal conductivity
C'	species concentration	ρ	fluid density
K'	permeability of porous medium		**Subscript**
Sc	Schmidt number	w	wall conditions
a'	absorption co-efficient of the medium	∞	free stream conditions

Appendix

$$h(\xi,z,t)=\frac{1}{2}\left[e^{\sqrt{\xi}z}\,erfc\left(\frac{z}{2\sqrt{t}}+\sqrt{\xi t}\right)+e^{-\sqrt{\xi}z}\,erfc\left(\frac{z}{2\sqrt{t}}-\sqrt{\xi t}\right)\right]$$

$$\psi(\beta,R\beta,z,t)=\frac{1}{2}\left[e^{\beta\sqrt{R}z}\,erfc\left(\frac{z}{2}\sqrt{\frac{\beta}{t}}+\sqrt{R\beta t}\right)+e^{-\beta\sqrt{R}z}\,erfc\left(\frac{z}{2}\sqrt{\frac{\beta}{t}}-\sqrt{R\beta t}\right)\right]$$

$$f(\beta,R\beta,z,t)=\left(\frac{t}{2}+\frac{z}{4}\sqrt{\frac{1}{R}}\right)e^{\beta\sqrt{R}z}\,erfc\left(\frac{z}{2}\sqrt{\frac{\beta}{t}}+\sqrt{R\beta t}\right)+\left(\frac{t}{2}+\frac{z}{4}\sqrt{\frac{1}{R}}\right)e^{-\beta\sqrt{R}z}\,erfc\left(\frac{z}{2}\sqrt{\frac{\beta}{t}}-\sqrt{R\beta t}\right)$$

$$F(\xi,z,t)=\frac{1}{2}\left[\left(t+\frac{1}{2}\sqrt{\frac{z}{\xi}}\right)e^{\sqrt{\xi}z}\,erfc\left(\frac{z}{2\sqrt{t}}+\sqrt{\xi t}\right)+\left(t-\frac{1}{2}\sqrt{\frac{z}{\xi}}\right)e^{-\sqrt{\xi}z}\,erfc\left(\frac{z}{2\sqrt{t}}-\sqrt{\xi t}\right)\right]$$

$$\hbar(\xi,t)=-\left[\frac{1}{\sqrt{\pi t}}e^{-\xi t}+\sqrt{\xi}\,erf\left(\sqrt{\xi t}\right)\right]$$

$$\hbar(\xi+i\omega,t)=-\left[\frac{1}{\sqrt{\pi t}}e^{-(\xi+i\omega)t}+\sqrt{(\xi+i\omega)t}\,erf\left(\sqrt{(\xi+i\omega)t}\right)\right]$$

$$\Omega(\beta,R\beta,t)=-\left[\sqrt{\frac{\beta}{\pi t}}\,e^{-\alpha t}+\beta\sqrt{R}\,erf\left(\sqrt{R\beta t}\right)\right]$$

$$\varphi(\beta,R\beta,t)=-\left[\sqrt{\frac{1}{4R}}\,erf\left(\sqrt{R\beta t}\right)+t\,\beta\sqrt{R}\,erf\left(\sqrt{R\beta t}\right)+\sqrt{\frac{t\beta}{\pi}}e^{-R\beta t}\right]$$

$$\Gamma(\xi,t)=-\left[\left(\frac{1}{2\sqrt{\xi}}+\sqrt{\xi}\,t\right)erf(\sqrt{\xi t})-\sqrt{\frac{t}{\pi}}\,e^{-\xi t}\right]$$

Conflict of Interest

The authors have no conflict of interest.

ORCID

Dibya Jyoti Saikia, https://orcid.org/0000-0001-6067-5390; **Nazibuddin Ahmed,** https://orcid.org/0000-0002-0924-4402
Richa Deb Dowerah, https://orcid.org/0009-0008-1220-8526; **Ardhendu Kumar Nandi,** https://orcid.org/0000-0002-4091-7994
Rajdeep Bordoloi, https://orcid.org/0000-0001-8508-8328

REFERENCES

[1] B. Alazmi, and K. Vafai, "Analysis of variable porosity, thermal dispersion, and local thermal nonequilibrium on free surface flows through porous media," J. Heat Transfer, **126**(3), 389-399 (2004). https://doi.org/10.1115/1.1723470
[2] M. Lahonian, S. Aminian, and M.S. Rahimi, "Study of MHD Mixed Convection of Different Nanofluids Due to the Inner Rotating Cylinder Saturated with Porous Media," Journal of The Institution of Engineers (India): Series C, **104**(1), 169-181 (2023). https://doi.org/10.1007/s40032-022-00903-y
[3] A. Haritha, B. Vishali, and C. Venkata Lakshmi, "Heat and mass transfer of MHD Jeffrey nanofluid flow through a porous media past an inclined plate with chemical reaction, radiation, and Soret effects," Heat Transfer, **52**(2), 1178-1197 (2023). https://doi.org/10.1002/htj.22735
[4] S. Jauhri, and U. Mishra, "Numerical investigation of MHD nanofluid considering second-order velocity slip effect over a stretching sheet in porous mediam," Journal of Integrated Science and Technology, **11**(2), 478-478 (2023). https://pubs.thesciencein.org/journal/index.php/jist/article/view/478
[5] M.V. Krishna, M.G. Reddy, and A.J. Chamkha, "Heat and mass transfer on unsteady MHD flow through an infinite oscillating vertical porous surface," Journal of Porous Media, **24**(1), 81-100 (2021). https://doi.org/10.1615/JPorMedia.2020025021
[6] S. Matta, G.R. Malga, B.S. Goud, L. Appidi, and P.P. Kumar, "Effects of viscous dissipation on MHD free convection flow past a semi-infinite moving vertical porous plate with heat sink and chemical reaction," Materials Today: Proceedings, **92**(Part 2), 1629-1636 (2023). https://doi.org/10.1016/j.matpr.2023.06.108
[7] N.H. Hamad, "Unsteady MHD natural convection flow past an infinite vertical porous plate with radiation absorption effects," Heat Transfer, **52**(2), 1345-1364 (2023). https://doi.org/10.1002/htj.22743
[8] J.K. Singh, G.S. Seth, and P. Rohidas, "Impacts of time varying wall temperature and concentration on MHD free convective flow of a rotating fluid due to moving free-stream with hall and ion-slip currents," International Journal of Thermofluid Science and Technology, **6**(3), 19060301 (2019). https://doi.org/10.36963/IJTST.19060301
[9] H.A. Nabwey, A.M. Rashad, P.B.A. Reddy, S. Jakeer, M.A. Mansour, and T. Salah, "Radiative effects on unsteady MHD natural convection flow in an inclined wavy porous cavity using hybrid nanofluid containing a square obstacle," Alexandria Engineering Journal, **65**, 921-937 (2023). https://doi.org/10.1016/j.aej.2022.10.004
[10] T. Saha, T. Islam, S. Yeasmin, and N. Parveen, "Thermal influence of heated fin on MHD natural convection flow of nanofluids inside a wavy square cavity," International Journal of Thermofluids, **18**, 100338 (2023). https://doi.org/10.1016/j.ijft.2023.100338
[11] D.J. Saikia, N. Ahmed, and R. Bordoloi, "Natural Convective MHD Mass Transfer Flow Past an Infinite Vertical Porous Plate Embedded in a Porous Medium with Thermal Diffusion and Chemical Reaction," Special Topics & Reviews in Porous Media: An International Journal, **14**(2), 63-75 (2023). https://doi.org/10.1615/SpecialTopicsRevPorousMedia.2023045885
[12] B.S. Goud, Reddy, Y.D. Reddy, and K.K. Asogwa, "Chemical reaction, Soret and Dufour impacts on magnetohydrodynamic heat transfer Casson fluid over an exponentially permeable stretching surface with slip effects," International Journal of Modern Physics B, **37**(13), 2350124 (2023). https://doi.org/10.1142/S0217979223501242
[13] P.R. Sekhar, S. Sreedhar, S.M. Ibrahim, and P.V. Kumar, "Radiative Heat Source Fluid Flow of MHD Casson Nanofluid over A Non-Linear Inclined Surface with Soret and Dufour Effects," CFD Letters, **15**(7), 42-60 (2023). https://doi.org/10.37934/cfdl.15.7.4260
[14] A.R. Deepika, K. Govardhan, A. Rana, and M. Reza, "Soret and Dufour effects on MHD mixed convection flow of Casson hybrid nanofluid over a permeable stretching sheet," International Journal of Ambient Energy, **44**(1), 2115-2127 (2023). https://doi.org/10.1080/01430750.2023.2224337
[15] K. Choudhuri, N. Ahmed, and P.J. Parashar, "Soret and Dufour Effects in A Three-Dimensional Mhd Flow Past a Semi-Infinite Uniformly Moving Vertical Plate with Constant Heat Flux: Soret and Dufour effects in a three-dimensional MHD flow," Latin American Applied Research-An international journal, **53**(3), 263-270 (2023). https://doi.org/10.52292/j.laar.2023.1000
[16] Y.D. Reddy, and B.S. Goud, "Comprehensive analysis of thermal radiation impact on an unsteady MHD nanofluid flow across an infinite vertical flat plate with ramped temperature with heat consumption," Results in Engineering, **17**, 100796 (2023). https://doi.org/10.1016/j.rineng.2022.100796
[17] S.G. Bejawada, and M.M. Nandeppanavar, "Effect of thermal radiation on magnetohydrodynamics heat transfer micropolar fluid flow over a vertical moving porous plate," Experimental and Computational Multiphase Flow, **5**(2), 149-158 (2023). https://doi.org/10.1007/s42757-021-0131-5
[18] E.A. Algehyne, S.A. Lone, Z. Raizah, S.M. Eldin, A. Saeed, and A.M. Galal, "Analysis of the electrically conducting magnetohydrodynamic hybrid nanofluid flow past a convectively heated stretching surface with suction/injection and non-linear thermal radiation," Frontiers in Materials, **10**, 1132124 (2023). https://doi.org/10.3389/fmats.2023.1132124
[19] C.M. Koli, and S.N. Salunkhe, "Thermal Radiation and Magnetic Fields Effects on Nanofluids flowing through Stretch Sheet," Journal of Computational Applied Mechanics, **54**(1), 111-126 (2023). https://doi.org/10.22059/jcamech.2023.353492.791
[20] N. Vijay, and K. Sharma, "Entropy generation analysis in MHD hybrid nanofluid flow: Effect of thermal radiation and chemical reaction," Numerical Heat Transfer, Part B: Fundamentals, **84**(1), 66-82 (2023). https://doi.org/10.1080/10407790.2023.2186989
[21] D. Iranian, and S. Karthik, "Heat generation effects on Magnetohydrodynamic Powell-Eyring fluid flow along a vertical surface with a Chemical reaction," Forces in Mechanics, **12**, 100212 (2023). https://doi.org/10.1016/j.finmec.2023.100212
[22] N.F.M. Omar, H.I. Osman, A.Q. Mohamad, R. Jusoh, and Z. Ismail, "Analytical Solution of Unsteady MHD Casson Fluid with Thermal Radiation and Chemical Reaction in Porous Medium," Journal of Advanced Research in Applied Sciences and Engineering Technology, **29**(2), 185-194 (2023). https://doi.org/10.37934/araset.29.2.185194

[23] B.P. Reddy, M.H. Simba, and A. Hugo, "Effects of Thermodiffusion and Chemical Reaction on Magnetohydrodynamic-Radiated Unsteady Flow Past an Exponentially Accelerated Inclined Permeable Plate Embedded in a Porous Medium," International Journal of Chemical Engineering, **2023**, 9342174 (2023). https://doi.org/10.1155/2023/9342174

[24] L. Appidi, P.P. Kumar, S. Matta, and B.S. Malga, "Effects of chemical reaction and thermal radiation on MHD free convective flow of micro polar fluid past an infinite moving vertical porous plate with viscous dissipation," Heat Transfer, **52**(3), 2922-2939 (2023). https://doi.org/10.1002/htj.22811

ТОЧНИЙ АНАЛІЗ ДИФУЗІЙНО-ТЕРМОЕФЕКТУ НА МГД ПРИРОДНИЙ КОНВЕКТИВНИЙ ПОТОК ПОВЗ КОЛИВАЛЬНУ ВЕРТИКАЛЬНУ ПЛАСТИНИ З ХІМІЧНОЮ РЕАКЦІЄЮ ТА ТЕПЛОВИМ ВИПРОМІНЮВАННЯМ У ПОРИСТОМУ СЕРЕДОВИЩІ

Діб'я Джіоті Сайкія[a], Назібуддін Ахмед[b], Річа Деб Доверах[c], Ардхенду Кумар Нанді[a], Раджділ Бордолой[d], Харун Аль Рашид[e]

[a]Департамент математики, Басугаон коледж, Басугаон, BTR, Чіранг, 783372, India
[b]Департамент математики Університет Коттон, Гувахаті, 781001, Індія
[c]Департамент математики, Університет Гаухаті, Гувахаті, Ассам, 781014, Індія
[d]Департамент математики, Сібсагарський університет, Сібсагар, Ассам, 785640, Індія
[e]Департамент математики, Біласіпара коледж, Біласіпара, 783348, Індія

Основна мета цього дослідження полягає в дослідженні впливу дифузії-термо на характеристики потоку МГД природної конвекції через проникне середовище повз безкінечно осцилюючу вертикальну пластину, враховуючи хімічну реакцію та ефекти теплового випромінювання. Підхід перетворення Лапласа використовується для вирішення керівних рівнянь для рівняння безперервності видів, енергії та імпульсу. Результати моделювання показують, що теплове випромінювання збільшує первинну швидкість рідини, одночасно зменшуючи вторинну швидкість рідини. Крім того, збільшення числа Дюфура (Du) призводить до більш високих температурних полів, а також до збільшення первинної та вторинної швидкостей рідини. Також дифузійно-термальний ефект сприяє поліпшенню температурного поля. Отримано рівняння шкірного тертя, яке показано графічно. Для демонстрації чисел Нуссельта та Шервуда використовуються тривимірні графіки поверхні. Крім того, графічні зображення використовуються для зображення впливу безрозмірних факторів на концентрацію, температуру та моделі швидкості.

Ключові слова: *вільна конвекція; пористе середовище; дифузійно-термальний; хімічна реакція; теплове випромінювання*